ZAMM · Z. Angew. Math. Mech. **85**, No. 9, 607 – 617 (2005) / **DOI** 10.1002/zamm.200410208

Microarchitectured cellular solids – the hunt for statically determinate periodic trusses

Plenary lecture presented at the 75th Annual GAMM Conference, Dresden, Germany, 22–26 March 2004

R. G. Hutchinson and N. A. Fleck*

Cambridge University Engineering Dept., Trumpington St., Cambridge, CB2 1PZ, UK

Received 10 June 2004, revised and accepted 15 December 2004
Published online 10 June 2005

Key words cellular solids, statically determinate, actuation, Kagome, octet truss, double-layer grid
MSC (2000) 74M25

The mechanical properties of open-cell metallic foams and periodic lattice materials are explained by a structural analysis of their parent pin-jointed truss structures. A matrix method of analysis is presented in order to elucidate whether a periodic truss structure can collapse by macroscopic strain producing mechanisms, or by periodic collapse mechanisms which induce zero macroscopic strain to first order. It is shown that the planar Kagome truss is of the latter type, and is consequently stiff. The in-plane stiffness of the 2D Kagome grid and the bending stiffness of the 3D Kagome double-layer grid (KDLG) are determined for elastic members. An alternative, statically determinate, double-layer grid is derived from the octet truss, and is referred to as the modified octet truss (MOT). This structure has faces comprising a hexagonal grid and a semi-regular triangular grid, and is much less stiff than the Kagome double-layer grid. Both structures have morphing capability due to their static and kinematic determinacy.

1 Introduction

Cellular solids of low relative density can be considered to have the microarchitecture of an assembly of welded struts. The recent study of Deshpande, Ashby, and Fleck [4,5] reveals that the macroscopic properties are largely dictated by the connectivity of joints rather than by the regularity of the microstructure. Consider the case of open-cell metallic foams, as reviewed by Ashby et al. [1]. They are manufactured mostly from the melt by the expansion of gas bubbles, and the expansion process is driven by the minimisation of surface energy. Consequently, they have microstructures which, although stochastic, have a low nodal connectivity of 3–4 adjoining bars per joint. (The parent pin-jointed structure contains collapse mechanisms.) The stiffness and strength of these 3D structures relies upon the bending stiffness of the bars, and they are consequently referred to as *bending dominated structures*. Define the relative density $\bar{\rho}$ as the ratio of the density of the porous solid to that of the solid from which it is derived. Then, it follows by straightforward beam-bending theory and dimensional analysis that the Young's modulus E of open-cell foams scales with that of the fully dense solid E_S according to $E \approx \bar{\rho}^2 E_S$. The yield strength σ_Y scales with $\bar{\rho}$ and with the yield strength of the parent solid σ_{YS} according to $\sigma_Y \approx 0.3\bar{\rho}^{3/2}\sigma_{YS}$. Both relations are supported by a wealth of experimental data, see Ashby et al. [1] and the recent conference proceedings edited by Banhart, Fleck, and Mortensen [2]. The recently developed lattice materials such as the octet truss have a nodal connectivity (co-ordination number) of 12 and are *stretching dominated structures*. These cellular solids have the virtue that the stiffness and strength scale linearly with the relative density and thereby out-perform metallic foams; their parent pin-jointed trusses are highly redundant. A variety of fabrication routes have evolved to construct these periodic lattices, see Wadley et al. [16].

There is increasing interest in the development of morphing materials which are stiff to external loads but have the ability to undergo large changes of shape upon actuation by lengthening (or shortening) some part of the material. One strategy for identifying useful morphing materials is to consider periodic, pin-jointed trusses.† If the pin-jointed structure is both *kinematically determinate* (no internal mechanisms) and *statically determinate* (no internal states of self-stress), it will be stiff to passive loads. Now replace one bar by an actuator and treat this actuator as external to the modified structure. The modified structure behaves as a mechanism with a single degree of freedom, and this mechanism is activated by elongation of

* Corresponding author, e-mail: naf1@eng.cam.ac.uk, phone: +44 (0)1223 332650, fax: +44 (0)1223 332662

† Throughout this paper, properly arranged external constraints (3 for 2D trusses and 6 for 3D space trusses) are applied. They provide a statically determinate support for a rigid body: A rigid body with these constraints forms a statically determinate structure.

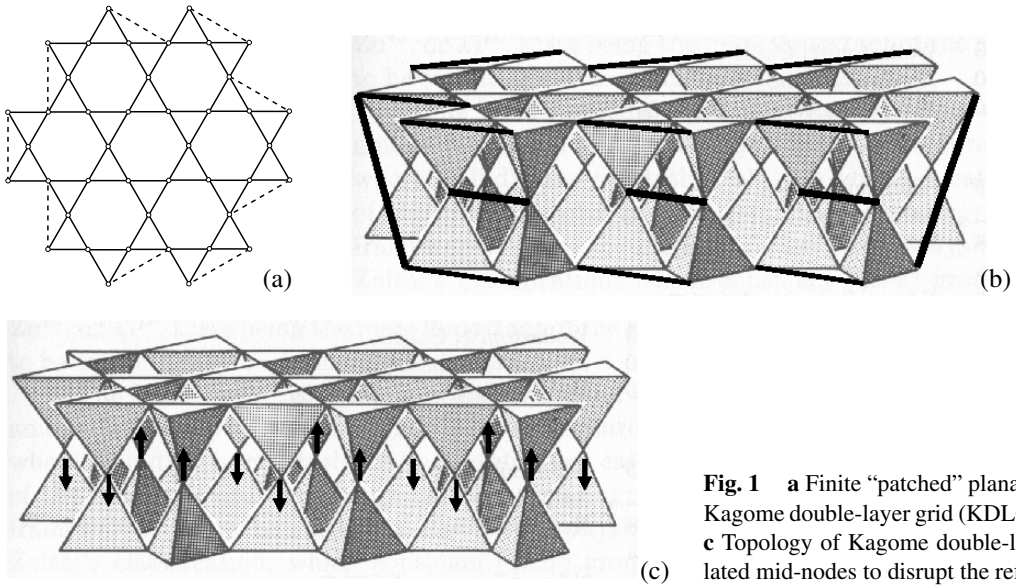

Fig. 1 **a** Finite "patched" planar Kagome grid. **b** Topology of Kagome double-layer grid (KDLG) including patching scheme. **c** Topology of Kagome double-layer grid (KDLG) with translated mid-nodes to disrupt the reflective symmetry.

the actuator. It is anticipated that the rigid-jointed version of a statically and kinematically determinate pin-jointed structure will inherit a morphing capability.

The hunt for a periodic, statically and kinematically determinate, 2D or 3D structure is a challenging task. Recently, Guest and Hutchinson [6] have proved that no such infinite periodic structure exists. However, we shall show that *finite* versions of periodic 2D and 3D structures can be made statically and kinematically determinate by minor modifications. For example, the finite planar Kagome grid, with suitable patch bars on the periphery, is both statically and kinematically determinate, see Fig. 1a. The pin-jointed version of the finite Kagome double-layer grid (KDLG), with peripheral patch bars as shown in Fig. 1b, contains states of self-stress. However, the structure can be made statically and kinematically determinate by a symmetry breaking operation: The position of the mid-plane nodes are perturbed to introduce asymmetry, see Fig. 1c. The double-layer grid exists as a plate-like structure, or can be distorted into a shell-like structure with single or double curvature, as discussed by Symons et al. [15]. An alternative statically and kinematically determinate double-layer lattice is introduced in this paper: The *modified octet truss* (MOT). Recall that the parent (3D) octet truss is near optimal in stiffness but is redundant due to its high average connectivity of 12. Thus the question arises: How can the octet truss be modified to a statically and kinematically determinate form? We address this question below, and then derive the properties of the modified octet truss. The main finding is that the modified octet truss is much less stiff in axial extension and in bending than the Kagome double-layer grid.

2 Matrix analysis of periodic truss structures

We begin by considering the equilibrium and kinematics of periodic pin-jointed trusses with extensional bars, in terms of the matrix methods developed by Pellegrino and Calladine [12]. A truss is *statically determinate* when the tension in every bar can be determined *solely* from the equilibrium equations for a given set of external force components applied to each joint (or node); the number of equations is equal to the number of unknowns. A truss is *kinematically determinate* if the location of each joint is uniquely determined by the length of each bar. We first introduce the *equilibrium matrix* $\boldsymbol{A}$. Consider a planar truss (dimension $N = 2$) or a spatial truss (dimension $N = 3$) consisting of j total joints connected by b bars and constrained by k *kinematic constraints* to rigid foundations. Then, one can identify the following static and kinematic variables: b bar *tensions* assembled into a vector $\boldsymbol{t}$, $Nj - k$ components of *external force* assembled into the vector $\boldsymbol{f}$, b bar *elongations* assembled into the vector $\boldsymbol{e}$, and $Nj - k$ *displacement* components assembled into the vector $\boldsymbol{d}$. Joint equilibrium dictates the matrix relation

$$\boldsymbol{A} \cdot \boldsymbol{t} = \boldsymbol{f} \tag{1}$$

between bar tensions and joint forces, in terms of a rectangular equilibrium matrix $\boldsymbol{A}$, of dimension $Nj - k$ by b. Similarly, compatibility of bar extensions and joint displacements dictates that

$$\boldsymbol{B} \cdot \boldsymbol{d} = \boldsymbol{e} \tag{2}$$

where the *kinematic matrix* $\boldsymbol{B}$ is of dimension b by $Nj - k$. Straightforward application of the principle of virtual work reveals that $\boldsymbol{A}$ and $\boldsymbol{B}$ are connected directly by $\boldsymbol{B} = \boldsymbol{A}^{\mathrm{T}}$ where the superscript T denotes the transpose.

To generalise Maxwell's rule, Pellegrino and Calladine [12] derived the following relations:

$$s = b - r_A \tag{3}$$

$$m = Nj - k - r_A \tag{4}$$

where $s \geq 0$ is the number of independent *states of self-stress*, r_A is the *rank* of the equilibrium matrix $\boldsymbol{A}$ (denoted rank($\boldsymbol{A}$)), $m \geq 0$ is the number of independent inextensional *mechanisms*, j is the total number of joints, and k is the number of kinematic constraints to a rigid foundation. Note that s can be qualitatively described as the number of redundant bars (see [3, 12]). The relations (3) and (4) may be justified through examination of the four fundamental subspaces of $\boldsymbol{A}$: $\mathrm{Row}(\boldsymbol{A})$, $\mathrm{Col}(\boldsymbol{A})$, $\mathrm{Nul}(\boldsymbol{A})$, and $\mathrm{Nul}\big(\boldsymbol{A}^{\mathrm{T}}\big)$, see for example Strang [14]. Pellegrino and Calladine [12] give the following interpretation to these subspaces:

1. $\mathrm{Row}(\boldsymbol{A})$: basis for the equilibrium bar tension vectors $\boldsymbol{t}$ without self-stress, with dimension $\dim(\mathrm{Row}(\boldsymbol{A})) = r_A$. Kinematically, this subspace is composed of all geometrically compatible bar elongations $\boldsymbol{e}$ since $\mathrm{Row}(\boldsymbol{A}) = \mathrm{Col}(\boldsymbol{B})$.
2. $\mathrm{Col}(\boldsymbol{A})$: basis for the equilibrium external force vectors without self-stress $\boldsymbol{f}$ where $\dim(\mathrm{Col}(\boldsymbol{A})) = r_A$. Kinematically, this subspace is composed of all geometrically compatible joint displacements $\boldsymbol{d}$ since $\mathrm{Col}(\boldsymbol{A}) = \mathrm{Row}(\boldsymbol{B})$.
3. $\mathrm{Nul}(\boldsymbol{A})$: basis for all bar tensions $\boldsymbol{t}$ in equilibrium with $\boldsymbol{f} = \boldsymbol{0}$. This comprises all the states of self-stress, with $\dim(\mathrm{Nul}(\boldsymbol{A})) = b - r_A = s$. Kinematically, this subspace is composed of all geometrically incompatible $\boldsymbol{e}$ since $\mathrm{Nul}(\boldsymbol{A}) = \mathrm{Nul}\big(\boldsymbol{B}^{\mathrm{T}}\big)$.
4. $\mathrm{Nul}(\boldsymbol{A}^{\mathrm{T}})$: basis for the inadmissible external force vectors $\boldsymbol{f}$, with $\dim(\mathrm{Nul}(\boldsymbol{A}^{\mathrm{T}})) = Nj - k - r_A$. These force vectors are forbidden by the equilibrium equations. Kinematically, this subspace is composed of all geometrically incompatible $\boldsymbol{d}$, since $\mathrm{Nul}\big(\boldsymbol{A}^{\mathrm{T}}\big) = \mathrm{Nul}(\boldsymbol{B})$; this subspace is composed of all the inextensional mechanisms.

The above subspace interpretations lead directly to (3) and (4). Pellegrino [11] has recast the above items in terms of the singular value decomposition and has discussed the fundamental subspaces of several example trusses in detail.

2.1 Infinite periodic pin-jointed truss

For an infinite pin-jointed framework of connectivity Z and j joints, the total number of bars b is approximately $jZ/2$. Thus, the necessary, but not sufficient, condition for rigidity is $Z = 4$ in 2D and $Z = 6$ in 3D [4]. A Venn diagram to illustrate the various types of mechanism exhibited by classes of 2D periodic pin-jointed truss is given in Fig. 2. Consider the various structures in turn. The fully triangulated structure, comprising equilateral triangles with a nodal connectivity of $Z = 6$, is highly redundant and possesses no collapse mechanisms. In contrast, a triangular-triangular lattice, with unit cell shown in Fig. 2, collapses by a mechanism which leads to a macroscopic hydrostatic strain. Thus, this structure has zero macroscopic stiffness against this collapse mode. The Kagome microstructure, as sketched in Fig. 1a, has a connectivity of $Z = 4$ and has no strain-producing collapse mechanisms; it can only collapse by periodic mechanisms which do not produce a macroscopic strain. Consequently, it is rigid in all directions. The cases of the square lattice and the hexagonal lattice, with a connectivity of $Z = 4$ and $Z = 3$, respectively, are different. Each of these structures can collapse by macroscopic strain-producing mechanisms, and by periodic collapse mechanisms. A methodology has been developed by Hutchinson and Fleck [7] to

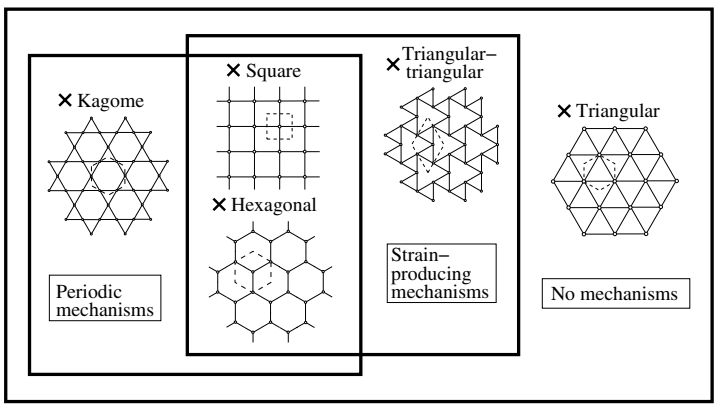

Fig. 2 Venn diagram of planar pin-jointed trusses.

explore the periodic collapse mechanisms based on Bloch-wave analysis; the details are beyond the scope of the present article. The main conclusion to draw from Fig. 2 is that the fully triangulated structure is macroscopically stiff because it possesses no collapse mechanisms while the Kagome structure is macroscopically stiff because it has only periodic collapse mechanisms which generate no macroscopic strain.

2.2 Exploration of strain-producing collapse mechanisms

Consider a periodic lattice, with n independent joints within each (primitive) unit cell. The entire lattice is constructed by translating the unit cell from the origin by a set of vectors $\boldsymbol{x}$. Let $\{\boldsymbol{j}_l\}$ be the joint basis used to define the relative location of each joint l within the unit cell. Then, the position vector of *any* joint throughout the lattice is $\boldsymbol{x}_l = \boldsymbol{j}_l + \boldsymbol{x}$ for joint number l. It is convenient to define the components of the various vectors in terms of the covariant basis $\{\boldsymbol{a}_\alpha\}$ of the direct lattice. Then, $\{\boldsymbol{a}^\alpha\}$ is the reciprocal lattice basis, $\alpha \in \{1, 2\}$.

The *Cauchy-Born hypothesis* states that a macroscopic, homogeneous displacement field $\boldsymbol{d}$ of the joints of a planar, periodic lattice may be defined using its unit cell Y (with boundary ∂Y) as

$$\boldsymbol{d}\left(\boldsymbol{x}_l, \bar{\boldsymbol{\varepsilon}}\right) = \bar{\boldsymbol{\varepsilon}} \cdot \boldsymbol{x} + \boldsymbol{p}\left(\boldsymbol{j}_l\right) \quad \forall\, \boldsymbol{j}_l \in \partial Y \tag{5}$$

where $\boldsymbol{p}\left(\boldsymbol{j}_l\right)$ is a periodic function which repeats from one unit cell to the next, and $\bar{\boldsymbol{\varepsilon}}$ is the symmetric second-order *macroscopic*, *average*, or *effective strain tensor*. The basic notion is to explore the existence of the set of $\boldsymbol{p}\left(\boldsymbol{j}_l\right)$ and associated $\bar{\boldsymbol{\varepsilon}}$ for a given periodic truss. This is achieved by substituting (5) into (2), to obtain a relation of the form

$$\bar{\boldsymbol{B}} \cdot \bar{\boldsymbol{d}} = \bar{\boldsymbol{e}} \tag{6}$$

where the vector $\bar{\boldsymbol{d}}$ comprises a linear combination of the components of $\bar{\boldsymbol{\varepsilon}}$ and $\boldsymbol{p}\left(\boldsymbol{j}_l\right)$. The null space $\mathrm{Nul}\left(\bar{\boldsymbol{B}}\right)$ is composed of all the inextensional mechanisms associated with a macroscopic strain. For some of these collapse modes the magnitude of the macroscopic strain may vanish. We find that the planar Kagome grid has only collapse mechanisms which produce zero macroscopic strain [8]. Consequently, it is macroscopically rigid for the case of inextensional bars and has a finite macroscopic stiffness for the case of bars with finite axial compliance.

The static boundary conditions consistent with the assumed kinematics of (5) are that the *tractions* $\boldsymbol{\sigma} \cdot \boldsymbol{n}$ are opposite on opposite faces of the unit cell boundary ∂Y. Consider a general unit cell Y made up of j pin-joints and b truss members with only joints on the unit cell boundary ∂Y. Identify each of the p periodic joint pairs on ∂Y separated by translation vectors,

$$\hat{\boldsymbol{x}} = \hat{x}^\alpha \boldsymbol{a}_\alpha \quad \forall\, \hat{x}^\alpha \in \{-1, 0, 1\}\,. \tag{7}$$

We re-label one joint of each pair such that the two joint positions are $\boldsymbol{j}_q$ and $\boldsymbol{j}_q + \hat{\boldsymbol{x}}_q$. This may be expressed in terms of (applied) joint forces on the boundary ∂Y as

$$\boldsymbol{f}\left(\boldsymbol{j}_q + \hat{\boldsymbol{x}}_q\right) + \boldsymbol{f}\left(\boldsymbol{j}_q\right) = \boldsymbol{0} \quad \forall\, \boldsymbol{j}_q \in \partial Y\,. \tag{8}$$

The boundary conditions analogous to (8) for the case when *bars*, rather than joints, are "cut" by the unit cell boundary are

$$t\left(\boldsymbol{b}_q + \hat{\boldsymbol{x}}_q\right) - t\left(\boldsymbol{b}_q\right) = 0 \quad \forall\, \boldsymbol{b}_q \in \partial Y \tag{9}$$

where $t\left(\boldsymbol{b}_q\right)$ are bar tensions and $\left\{\boldsymbol{b}_q\right\}$ is the bar basis. Clearly, a combination of (8) and (9) may be applied when *both* bars and joints are on ∂Y.

3 The planar Kagome truss

We consider first a planar Kagome grid of n hexagons per side, and derive the required patching scheme. Such a grid contains $6n^2$ triangles, and therefore the number of bars is $b = 18n^2$. The number of joints (nodes) is $j = 9n^2 + 3n$. For a planar Kagome grid there are no states of self stress, $s = 0$. If we apply three constraints, $k = 3$, to prevent rigid body motions we may determine the number of mechanisms (and therefore the number of patch bars required) from the 2D version of Maxwell's equation

$$s - m = b - 2j + k$$

giving

$$m = 6n - 3\,.$$

Thus, for the planar 7-hexagon Kagome grid ($n = 2$) we require 9 patch bars. There remains an arbitrary choice in the location of the patch bars, but the arrangement shown in Fig. 1a is systematic and straightforward to generate. Consider the planar Kagome truss as sketched in Fig. 1a, with each truss bar made from a linear elastic solid of Young's modulus E_S. Hyun and Torquato [10] have shown that the elastic, infinite version has in-plane effective properties which are close to optimal, and attain the upper Hashin-Shtrikman bound. In the dilute limit, the in-plane Young's modulus E scales with the relative density $\bar{\rho}$ of the cellular solid according to

$$E = \tfrac{1}{3}\bar{\rho}E_S \tag{10}$$

and the Poisson's ratio is $\nu = 1/3$. Strikingly, this effective response is identical to that of the fully triangulated truss.

4 The Kagome double-layer grid (KDLG)

Fig. 3 shows a plan view of three KDLGs with a number of hexagons per side n equal to 1, 2, and 3. The finite asymmetric KDLG contains no states of self-stress ($s = 0$) and is therefore statically determinate. To make the structure kinematically determinate ($m = 0$) the remaining mechanisms must be "switched off" by a peripheral patching scheme. We may use the same approach to determine the number of patches required for the three dimensional KDLG as for the planar Kagome grid described above. Assume the KDLG has planar Kagome faces comprising a grid of n-by-n hexagons. The number of tetrahedra in the KDLG is $12n^2$. Therefore, the number of bars is

$$b = 72n^2$$

and the number of joints is

$$j = 24n^2 + 6n\,.$$

If we apply 6 constraints ($k = 6$), to prevent rigid body motions we then apply the three dimensional form of Maxwell's equation

$$s - m = b - 3j + k$$

to obtain

$$m - s = 18n - 6\,.$$

For the asymmetric KDLG we have $s = 0$ and therefore the number of required patch-bars is $18n - 6$ in order to make the structure kinematically determinate ($m = 0$). The patching scheme adopted is sketched in Fig. 1b. The scheme for the top and bottom faces and the mid-plane nodes closely resembles that sketched in Fig. 1a for the planar Kagome grid. Three additional patch bars complete the patching scheme and these bars connect the top and bottom layers of the KDLG.

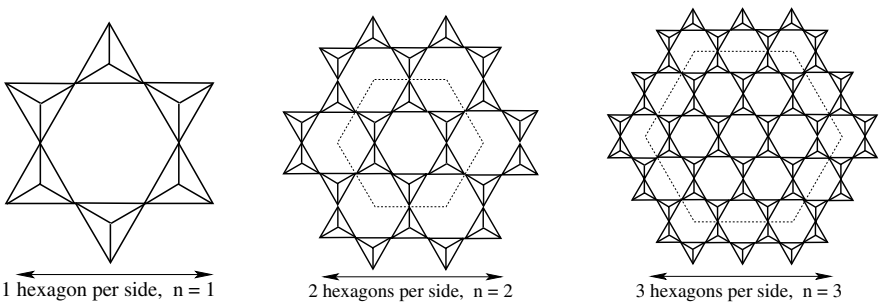

Fig. 3 Kagome double-layer grids (plan view).

4.1 Plate bending stiffness of the welded KDLG

The effective stretching stiffness $\bar{S}$ of the KDLG can be estimated by treating the structure as a sandwich with faces each of thickness t equal to that of the bar thickness, and a core of height H. Then, under a single component of axial force N

per unit width the effective plate stretching stiffness is simply $\bar{S} = 2S$, where $S = Et$ in terms of the effective Young's modulus E of the Kagome planar faces. Under a single component of applied moment, the plate bending stiffness is

$$\bar{D} = \tfrac{1}{2} S H^2 \,. \tag{11}$$

Substitution for (10) gives $\bar{D} = \frac{1}{6} t \bar{\rho} E_S H^2$. These expressions for the stretching and bending stiffness of the KDLG neglect the minor contribution from the bending stiffness of each bar. Note that the stiffnesses of the KDLG scale with relative density $\bar{\rho}$, implying a stretching response under all external loadings. We shall see that this response is in sharp contrast to that of the modified octet truss.

5 Modification of the octet truss to a statically and kinematically determinate design

Fig. 4b is a plan view of a finite octet-truss structure and Fig. 4a is a detail of the unit cell used to construct the octet-truss. The challenge is to convert this highly redundant pin-jointed structure to a statically and kinematically determinate form by suitable removal of bars. We first discuss the derivation of finite, pin-jointed, 2D statically and kinematically determinate structures that derive from the faces of the fully triangulated octet truss – the thick lines in Fig. 4. Consider the trial geometries detailed in Figs. 5a and 5b. Applying the matrix analysis development of Pellegrino and Calladine [12] in a MATLAB script, the equilibrium matrices ($\boldsymbol{A}$) for the structures of Fig. 5 were generated and rank($\boldsymbol{A}$) = r_A estimated. Then, the generalised Maxwell's rule for planar structures, $s = b - r_A$ and $m = 2j - r_A - 3$, was applied to each truss with the results quoted in Fig. 5; the most notable being that the truss of Fig. 5b is statically and kinematically determinate with $s = m = 0$. A larger example analogous to Fig. 5b is given in Fig. 6b for which $b = 101$, $j = 52$, and $r_A = 101 \Rightarrow s = m = 0$.

The algorithm developed to generate Fig. 6b and such frameworks of general size is as follows:

1. Translate the unit cell of Fig. 6a to generate a planar "network".
2. Add additional *boundary-layer* members, and joints if necessary, to render the planar truss statically and kinematically determinate. Use MATLAB or a similar mathematical programming environment (e.g. C, FORTRAN) to form the explicit equilibrium matrix $\boldsymbol{A}$, to estimate r_A, and thus numerically check that $s = m = 0$, upon evaluating $s = b - r_A$ and $m = 2j - r_A - 3$.

In progressing from Fig. 5a to 5b, the second step above involves the straightforward addition of three boundary bars. The complete construction of Fig. 6b requires the addition of eleven such bars.

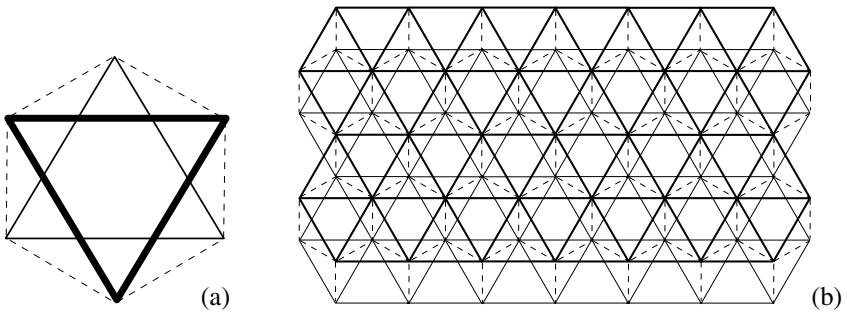

Fig. 4 **a** An octet unit cell, and **b** the corresponding octet truss, where thick solid, thin solid and dashed lines make up the top face, bottom face and core members respectively. All bars are of equal length.

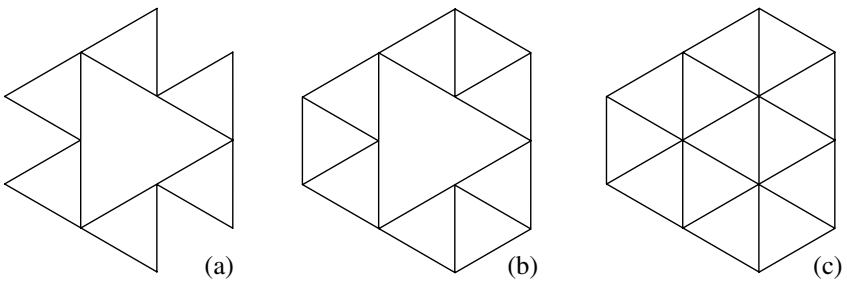

Fig. 5 Finite, planar trusses: **a** a mechanism ($s = 0, m = 3$); **b** statically and kinematically determinate ($s = m = 0$); and **c** a redundant fully triangulated truss ($s = 3, m = 0$).

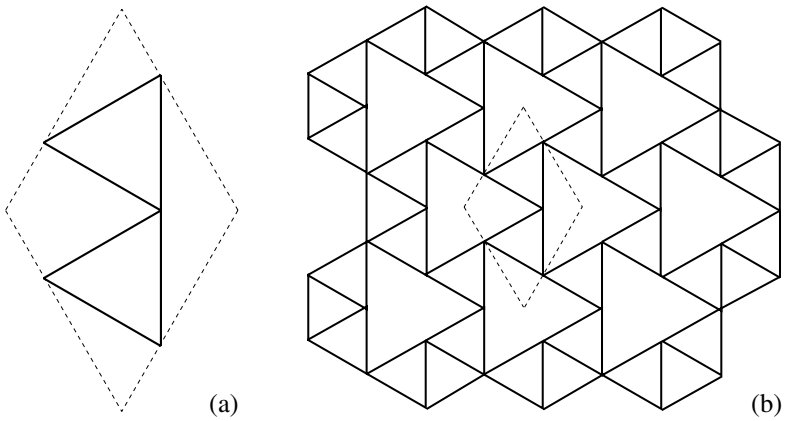

Fig. 6 **a** The triangle-triangle unit cell, and **b** a larger, statically and kinematically determinate version of Fig. 5b, with $b = 101$ and $j = 52$.

The unit cell given in Fig. 6a may be tessellated to form the infinitely periodic analog of Fig. 5a and was analysed using the matrix analysis techniques outlined above. After forming $\bar{\boldsymbol{A}} = \bar{\boldsymbol{B}}^{\mathrm{T}}$ (recall (6)), a MATLAB script was used to perform the following calculations. For each unit cell, the number of bars $b = 6$, the number of joints $j = 5$ and the number of periodic node pairs $p = 2 \Rightarrow \bar{\boldsymbol{A}}$ is a 6-by-6 real matrix. Finding that $\mathrm{rank}(\bar{\boldsymbol{A}}) = 4 \Rightarrow \dim(\mathrm{Nul}(\bar{\boldsymbol{A}})) = b - r_{\bar{A}} = 6 - 4 = 2$. This implies that $m = 1$ and the infinite truss is a *mechanism*. We thus find that this lattice cannot support biaxial loading. Fig. 6a satisfies the necessary rigidity condition that the average connectivity $Z = 4$ but not the sufficient condition, that $\dim(\mathrm{Nul}(\bar{\boldsymbol{A}})) = 3$.

5.1 Reduction of 3D octet truss to statically and kinematically determinate form

To identify a (finite) statically and kinematically determinate derivative of the octet truss, we adopted a trial and error method similar to that which generated Figs. 5a, 5b, and 6b. Fig. 7 summarises our early findings following a progression similar to that in Fig. 5. Applying the generalised Maxwell's rule to Fig. 7c one finds that $b = 69$ and $j = 22$ so $s - m = b - 3j + 6 = 69 - 66 + 6 = 9$. Using a MATLAB script to perform the required matrix computations, we find that rank($\boldsymbol{A}$) = 60, $s = b - r_A = 9$ and $m = 0$ as stated in Fig. 7. For Fig. 7b the corresponding data are: $b = 57$, $j = 21 \Rightarrow s - m = b - 3j + 6 = 57 - 63 + 6 = 0$ and $s = b - r_A = 57 - 57 = 0 \Rightarrow s = m = 0$ so this truss is statically and kinematically determinate. Fig. 7a is a mechanism with $b = 42$, $j = 18$, $s - m = -6$ and $r_A = 42$ so $s = 0$ and $m = 6$. A larger lattice of the type of Fig. 7b and its corresponding unit cell are detailed in Fig. 8. The structures of Figs. 7b and 8 are examples of what we call the *modified octet truss* (MOT). The construction recipe for Fig. 8b is similar to that given for Fig. 6b: First, tessellate a planar region with the unit cell and then affix additional *boundary-layer* members and joints about the perimeter of the lattice. The transition from Fig. 7a to 7b is the simplest example of the latter procedure which we shall term *octet addition* since one "completes" boundary octet units (as defined in Fig. 4a). As for Fig. 7b, the larger (pin-jointed) lattice of Fig. 8b may also be shown to be statically and kinematically determinate by inputing its joint coordinates and bar

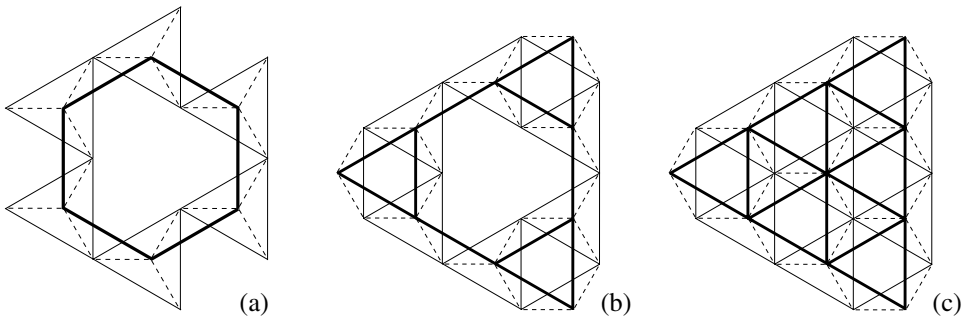

Fig. 7 Finite, spatial trusses based upon the octet truss: **a** a mechanism ($s = 0$, $m = 6$); **b** a statically and kinematically determinate truss ($s = m = 0$); and **c** the octet truss ($s = 9$, $m = 0$). The thick solid, thin solid and dashed lines represent the top face, bottom face and core members, respectively.

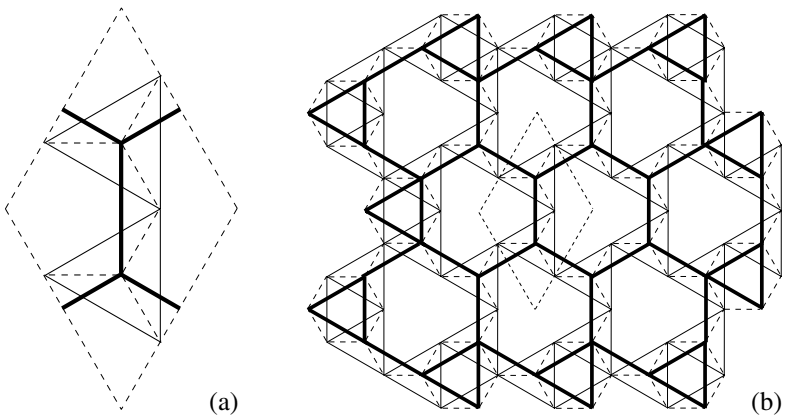

Fig. 8 **a** The modified octet truss unit cell and **b** a larger, statically and kinematically determinate variant of Fig. 7b. The thick solid, thin solid and dashed lines represent the top face, bottom face and core members, respectively.

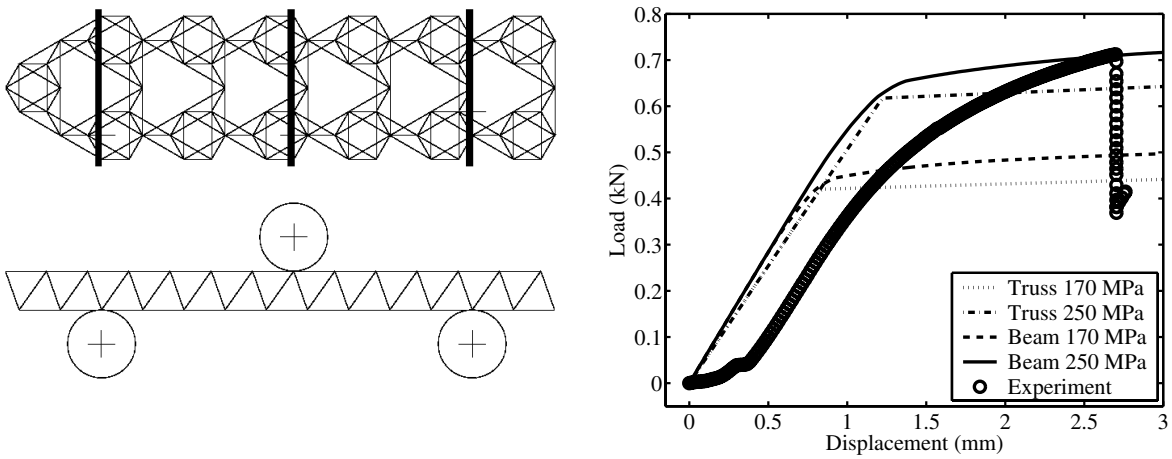

Fig. 9 Three point bending of a narrow ($n_W = 1$) modified octet truss beam. Comparison of ABAQUS finite element predictions and measured response, using truss or beam elements, and an assumed yield strength of 170 MPa or 250 MPa.

connectivity into the MATLAB script developed. Similarly, the unit cell of Fig. 8a is also a mechanism with $m = 3$, and these mechanisms are manifested as an inability to support biaxial in-plane loadings.

5.2 Three-point bending experiments on the modified octet truss

Test specimens were prepared by investment casting with the aluminium alloy LM25 (Al-Si 7-Mg 0.3 wt%). The finite lattices were composed of uniform members of radius 1 mm and length 14 mm (joint to joint). For brevity, we shall discuss here only one such lattice beam: A "narrow", finite MOT with width $n_W = 1$ and length $n_L = 6$, as measured in terms of unit cell multiples, and shown in Fig. 9. Thus, this lattice beam was approximately 130 mm long, 42 mm wide, and 12 mm high. The aluminium casting alloy had almost an elastic-perfectly plastic response with an elastic modulus E = 70 GPa and shortly after manufacture the measured yield strength was σ_Y = 170 MPa. The MOT lattice beam shown was loaded in three-point bending using 20 mm diameter steel rollers and a cross-head displacement rate of 1 mm per minute. The outer rollers were 108 mm (9 "bottom" joints) apart while the top loading roller was centred on a top joint equidistant between the outer supports. The load on the centre roller was measured using a 10 kN load cell and the corresponding displacement was measured using a linear voltage-displacement transducer.

5.2.1 Results

The transverse load versus displacement response (measured at the centre roller) of the MOT beam is plotted in Fig. 9. The specimen gave an initial non-linear response due to bedding-in of the rollers across the specimen width. The subsequent response was linear, followed by plastic yielding across the mid-section. This was confirmed by post-test examination: The specimen hinged at mid-span. This mode of plastic deformation is termed "face yield" as it involves plastic bending of the

section directly beneath the centre roller at the location of greatest effective bending moment. The final phase of deformation involved tensile fracture of the cast Al-alloy struts on the tensile, bottom face directly opposite the centre roller.

5.2.2 Three-point bending simulations

We modelled the modified octet-truss (MOT) of Fig. 9 using the ABAQUS finite element analysis package with both truss (pin-joints, T3D2) and Timoshenko beam (rigid-joints, B32) elements. The finite element analysis gave quantitative estimates for the three-point bending stiffness and limit load to compare directly with experiment. Fig. 9 shows the comparison of the ABAQUS analysis and the three-point bend experiment for this "narrow" MOT beam modelled using an assumed elastic-perfectly plastic response. The measured limit load is considerably larger than the prediction assuming $\sigma_Y = 170$ MPa. We also obtained predictions using $\sigma_Y = 250$ MPa. The measured collapse load lay between the predictions using truss elements and using Timoshenko beam elements. The beam elements are more appropriate due to the relatively stubby constituent members while the initial, elastic, transverse load-displacement slope is well-fit using either beam or truss elements. The limit load discrepancy for the choice $\sigma_Y = 170$ MPa is likely due to precipitation hardening of the as-received LM25 aluminium casting alloy at room temperature; subsequent Vickers hardness testing confirmed the choice of σ_Y = 250 MPa. The initial, experimental, elastic three-point bending behaviour is captured despite slight bedding-in effects (i.e. the displacement offset) using either truss or beam elements. The experimentally observed sudden load drop at around 2.7 mm transverse displacement is due to tensile fracture of highly-stressed bottom face sheet members immediately below the central roller. This load drop is *not* captured in our simulations as tensile fracture of the brittle cast-alloy struts was not addressed.

6 Effective properties of the modified octet truss

A series of finite element calculations have been performed by Hutchinson [8] to determine the bending stiffness of the modified octet truss (MOT). These calculations reveal that the MOT has a much lower bending stiffness than that of the KDLG. This is because the MOT relies for its stiffness upon the peripheral patch bars. In the absence of these patch bars the pin-jointed structure is a mechanism and the welded structure behaves as a bending dominated structure. Accurate estimates of the plate stretching stiffness $\bar{S}$ and the plate bending stiffness $\bar{D}$ are obtained by treating the MOT as a rigid-jointed sandwich structure, with a triangular-triangular face sheet and a hexagonal face sheet. The triangular-triangular face sheet deforms by bending of the struts, and elementary beam theory provides the effective Young's modulus as

$$E_{TT} = \tfrac{9}{32}\bar{\rho}^3 E_S \tag{12}$$

with a Poisson ratio $\nu = -1$. Similarly, the hexagonal faces deform by strut bending, and the effective Young's modulus is

$$E_H = \tfrac{3}{2}\bar{\rho}^3 E_S \tag{13}$$

with a Poisson ratio $\nu = 1$. The stretching stiffness $\bar{S}$ of the MOT can be estimated by treating the structure as a sandwich with faces each of thickness t equal to that of the bar thickness, and a core of height H. Then, under a single component of axial force N per unit width, the plate stretching stiffness is simply $\bar{S} = t\,(E_{TT} + E_H)$ in terms of the effective Young's moduli of the faces. Under a single component of applied moment, the effective plate bending stiffness is

$$\bar{D} = \frac{H^2}{2}\,\frac{(tE_{TT})^2 + (tE_H)^2}{t\,(E_{TT} + E_H)}\,. \tag{14}$$

Note that the stiffnesses of the MOT scale with relative density $\bar{\rho}^3$, implying a bending response under all external loadings.

7 Actuation of the MOT

The pin-jointed MOT is statically and kinematically determinate so, consequently, if one lengthens or shortens any individual constituent bar, *no* strain energy is stored during activation of this infinitesimal mechanism. Even when actuation of a bar is not infinitesimal, one would still expect little structural strain energy increase. This conclusion is moderated for the case of the rigid-jointed MOT as actuation will now lead to the storage of strain energy within the lattice. Further, constituent slender lattice members may yield or buckle. To investigate this idea, we simulated the actuation of four pin-jointed "actuators" (bars) in a MOT beam otherwise composed of either truss (T3D2) or Timoshenko beam (B32) elements modelling the lattice members; 1 mm in radius and 14 mm in length, as elastically-perfectly plastic with elastic modulus E = 70 GPa and yield strength σ_Y = 150 MPa. The actuators were strained via thermal expansion (T3D2T elements). When truss elements were used for the entire lattice, *all* the MOT members remained unloaded regardless of actuation strain. However, when

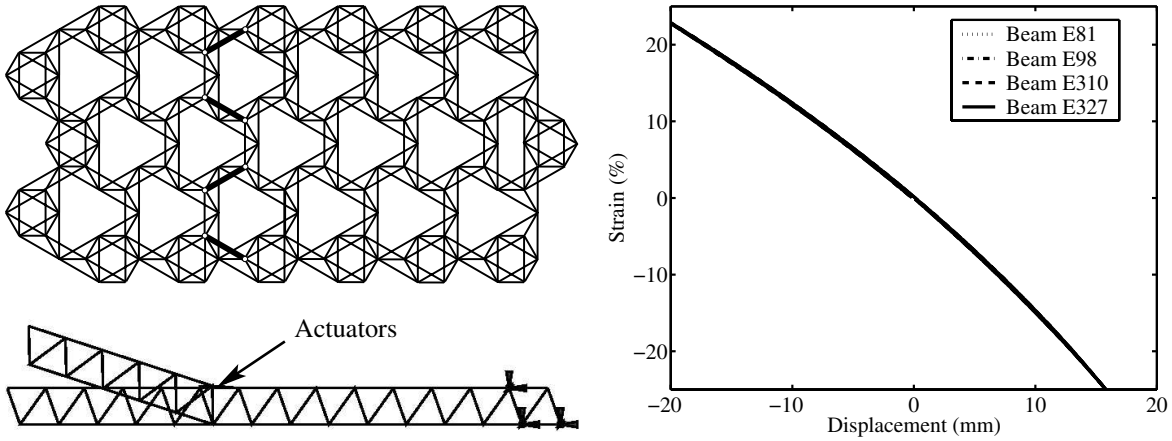

Fig. 10 ABAQUS actuation simulation wherein four top (hexagonal) face sheet members, shown in bold, are lengthened and contracted using thermal expansion (modelled as T3D2T truss elements). The MOT beam is fixed at one end such that when the actuating members contract the free end rises and when they expand the free end drops. The actuation strain of all four pin-jointed actuators is plotted versus the free-end, transverse displacement assuming the MOT is otherwise modelled using Timoshenko (B32) beam elements.

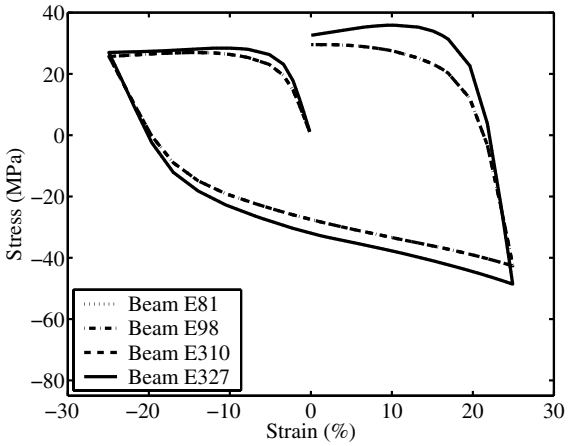

Fig. 11 Plot of the actuator stresses versus actuator strains corresponding to the strain-displacement plot of Fig. 10.

the passive MOT members were modelled as Timoshenko beams, the actuators and various bars and joints experienced significant stresses. Fig. 10 details the geometry ($n_W = 2$, $n_L = 6$) analysed and the actuation strain-transverse end displacement "waveform". Fig. 11 shows how the actuator stresses vary with actuator strain when the surrounding MOT is modelled using beam (rigid-jointed) elements.

The interpretation of Fig. 11 is as follows. The actuators remain elastic while several adjoining bars yield during actuator elongation and contraction. Consequently, in the physical realisation, one would expect that they would soon fail by low cycle fatigue. An additional parametric study is needed to explore the achievable actuation strain without inducing yield or buckling of the structure. It is expected that the achievable strain is sensitive to the slenderness ratio of the constituent lattice members. This has been explored for the case of the Kagome double-layer grid in the recent study of Symons et al. [15].

8 Concluding remarks

This study reveals that the modified octet truss (MOT) and the Kagome double-layer grid (KDLG) are each derived from statically and kinematically determinate pin-jointed parent structures. However, they have remarkably different structural behaviours. The MOT has a low, effective bending stiffness that may be attributed to the fact that much of the structure behaves as a mechanism with boundary bars required to make the structure statically and kinematically determinate. Consequently, the MOT is not as attractive a morphing material as the KDLG. Double-layer grids such as the MOT have a variety of possible actuation modes, with the maximum achievable actuation strain limited by yield or buckling of the rigid-jointed structure. The full range of morphing capability of double-layer grids (and fully 3D grids) remains an open issue.

Acknowledgements The authors are grateful for the financial support from a DARPA grant on synthetic multifunctional materials.

References

[1] M. F. Ashby, A. G. Evans, N. A. Fleck, L. J. Gibson, J. W. Hutchinson, and H. N. G. Wadley, Metal Foams: A Design Guide (Butterworth-Heinemann, Boston, 2000).
[2] J. Banhart, N. A. Fleck, and A. Mortensen (eds.), Proceedings of Metfoam 2003 Cellular Metals: Manufacture, Properties, Applications, Technical University of Berlin, 23–25 June 2003 (Verlag MIT Publishing, Berlin, 2003).
[3] C. R. Calladine, Int. J. Solids Struct. **14**, 161–172 (1978).
[4] V. S. Deshpande, M. F. Ashby, and N. A. Fleck, Acta Materialia **49**, 1035–1040 (2001).
[5] V. S. Deshpande, N. A. Fleck, and M. F. Ashby, J. Mech. Phys. Solids **49**(8), 1747–1769 (2001).
[6] S. D. Guest and J. W. Hutchinson, J. Mech. Phys. Solids **51**, 383–391 (2003).
[7] R. G. Hutchinson, Mechanics of Lattice Materials, Ph.D. thesis, Cambridge University (2004).
[8] R. G. Hutchinson and N. A. Fleck, The Mechanics of the Planar Kagome Truss, Manuscript in preparation (2004).
[9] R. G. Hutchinson, N. Wicks, A. G. Evans, N. A. Fleck, and J. W. Hutchinson, Int. J. Solids Struct. **40**, 6969–6980 (2003).
[10] S. Hyun and S. Torquato, J. Mater. Res. **7**, 137–144 (2002).
[11] S. Pellegrino, Int. J. Solids Struct. **30**, 3025–3035 (1993).
[12] S. Pellegrino and C. R. Calladine, Int. J. Solids Struct. **22**, 409–428 (1986).
[13] S. L. dos Santos e Lucato, J. Wang, P. Maxwell, R. M. McMeeking, and A. G. Evans, Int. J. Solids Struct. **41**, 3521–3543 (2004).
[14] G. Strang, Linear Algebra and Applications, third ed. (Wellesley-Cambridge Press, 2003).
[15] D. D. Symons, R. G. Hutchinson, and N. A. Fleck, J. Mech. Phys. Solids, in press (2005).
[16] H. N. G. Wadley, N. A. Fleck, and A. G. Evans, Compos. Sci. Technol. **63**, 2331–2343 (2003).

Book Review

Susan Friedlander and Denis Serre (eds.), Handbook of Mathematical Fluid Dynamics, Elsevier, North-Holland, Hardbound, Vol. 2, 2003, XI, 614pp. USD 135.00, EUR 135.00, GBP 90.00, ISBN 0-444-51287-x; Vol. 3, 2004, XI, 674pp., USD 175.00, EUR 175.00, GBP 116.50, ISBN 0-444-51556-9

This Handbook is a collection of refereed articles written by some of the very best specialists in Mathematical Fluid Dynamics. The editors decided to restrict the contents to mathematical aspects of fluid dynamics, avoiding to a large extent the physical and numerical aspects. But the authors have been encouraged to describe the physical meaning of the mathematical questions and results. The Handbook consists of three volumes. Volume 1 has been reviewed in this Journal of Applied Mathematics and Mechanics (ZAMM), Vol. 84, 2004, p. 834. Now the remaining volumes 2 and 3 have been published. Volume 2 contains a wide range of material with the majority of articles addressing issues related to incompressible fluids. Volume 3 begins with two fundamental articles on the continuum concept and on the vortex patches problem. The remaining articles concentrate on the Navier-Stokes equations. The contents in detail are:

Volume 2: 1. Robert: Statistical hydrodynamics, 2. Brenier: Topics on hydrodynamics and volume preserving maps, 3. Shnirelman: Weak solutions of incompressible Euler equations, 4. Constantin: Near identity transformations for the Navier-Stokes equations, 5. Ben-Artzi: Planar Navier-Stokes equations: vorticity approach, 6. Babin: Attractors of Navier-Stokes equations, 7. Renardy and Renardy: Stability and instability in viscous fluids, 8. Friedlander and Lipton-Lifschitz: Localized instabilities in fluids, 9. Gilbert: Dynamo theory, 10. Dias and Iooss: Water-waves as a spatial dynamical system, 11. Groah, Temple and Smoller: Solving the Einstein equations by Lipschitz continuous metrics: shock waves in general relativity.

Volume 3: 1. Esposito and Pulvirenti: From particles to fluids, 2. Chemin: Two-dimensional Euler system and vortex patches problem, 3. Cannone: Harmonic analysis tools for solving the incompressible Navier-Stokes equations, 4. Grenier: Boundary layers, 5. Zumbrun: Stability of large-amplitude shock waves of compressible Navier.Stokes quations (with Appendix by Jenssen and Lyng), 6. Temam and Ziane: Some mathematical problems in geophysical fluid dynamics.

Articles with more physical aspects of fluid dynamics are those on stability and instability in viscous fluids, on dynamo theory and on water-waves as dynamical system (using "dynamical" arguments was developed in the 1980 s, pioneered by K. Kirchgässner). The article on boundary layers is dealing mainly with stability aspects.

This three volume Handbook provides a comprehensive overview of the fascinating variety of mathematics that arise from the study of fluid motion. Altogether 3388 references are cited. The Handbook will certainly become the standard work in Mathematical Fluid Dynamics.

Bochum **K. Gersten**